Available online at www.sciencedirect.com
ScienceDirect
Geochimica et Cosmochimica Acta 75 (2011) 3501–3513
Geochimica et Cosmochimica Acta
www.elsevier.com/locate/gca

Evidence for aqueous activity on comet 81P/Wild 2 from sulfide mineral assemblages in Stardust samples and CI chondrites

Eve L. Berger [a,*], Thomas J. Zega [b], Lindsay P. Keller [c], Dante S. Lauretta [a]

[a] *Lunar and Planetary Laboratory, University of Arizona, Tucson, AZ 85721, USA*
[b] *Naval Research Laboratory, Washington DC 20375, USA*
[c] *NASA Johnson Space Center, Houston, TX 77058, USA*

Received 15 October 2010; accepted in revised form 16 March 2011; available online 22 March 2011

Abstract

The discovery of nickel-, copper-, and zinc-bearing iron sulfides from comet 81P/Wild 2 (Wild 2) represents the strongest evidence, in the Stardust collection, of grains that formed in an aqueous environment. We investigated three microtomed TEM sections which contain crystalline sulfide assemblages from Wild 2 and twelve thin sections of the hydrothermally altered CI chondrite Orgueil. Detailed structural and compositional characterizations of the sulfide grains from both collections reveal striking similarities. The Stardust samples include a cubanite ($CuFe_2S_3$) grain, a pyrrhotite [$(Fe,Ni)_{1-x}S$]/pentlandite [$(Fe,Ni)_9S_8$] assemblage, and a pyrrhotite/sphalerite [(Fe,Zn)S] assemblage. Similarly, the CI-chondrite sulfides include individual cubanite and pyrrhotite grains, cubanite/pyrrhotite assemblages, pyrrhotite/pentlandite assemblages, as well as possible sphalerite inclusions within pyrrhotite grains. The cubanite is the low temperature orthorhombic form, which constrains temperature to a maximum of 210 °C. The Stardust and Orgueil pyrrhotites are the 4C monoclinic polytype, which is not stable above ~250 °C. The combinations of cubanite and pyrrhotite, as well as pyrrhotite and pentlandite signify even lower temperatures. The crystal structures, compositions, and petrographic relationships of these sulfides constrain formation and alteration conditions. Taken together, these constraints attest to low-temperature hydrothermal processing.

Our analyses of these minerals provide constraints on large scale issues such as: heat sources in the comet-forming region; aqueous activity on cometary bodies; and the extent and mechanisms of radial mixing of material in the early nebula. The sulfides in the Wild 2 collection are most likely the products of low-temperature aqueous alteration. They provide evidence of radial mixing of material (e.g. cubanite, troilite) from the inner solar system to the comet-forming region and possible secondary aqueous processing on the cometary body.

1. INTRODUCTION

In 2006, NASA's Stardust mission successfully achieved its goal of collecting cometary and interstellar particles from Wild 2 and returning them to Earth. The captured material has a diverse mineralogy, which includes olivines, pyroxenes, sulfides, and oxides (Zolensky et al., 2006). This mélange of minerals is evidence of a large degree of radial mixing in the early solar nebula. For example, the presence of refractory CAI-like components in the Stardust collection is evidence for mixing of material formed at high temperatures from close to the early Sun out to the comet-forming region (Zolensky et al., 2006). Complementary information about low-temperature processes is furnished by sulfide minerals, which are present in the Stardust collection (Zolensky et al., 2006).

There is a subset of minerals reported in the Stardust collection (e.g. Brownlee et al., 2006; Flynn et al., 2006; Zolensky et al., 2006; Wirick et al., 2007; Flynn et al., 2008; Zolensky et al., 2008a; Burchell and Kearsley, 2009; Flynn et al., 2009; Bridges et al., 2010; Stodolna et al., 2010) that is similar to those found in the CI-chondrite suite (e.g. Fitch

* Corresponding author.
E-mail address: elberger@lpl.arizona.edu (E.L. Berger).

0016-7037/$ - see front matter © 2011 Elsevier Ltd. All rights reserved.
doi:10.1016/j.gca.2011.03.026

et al., 1962; Kerridge and Chatterji, 1968; Kerridge, 1970; Macdougall and Kerridge, 1977; Kerridge et al., 1979; Kerridge et al., 1980; Fredriksson and Kerridge, 1988; Bullock et al., 2005; Zolensky et al., 2008b) including carbonates ($[CaMg(CO_3)_2]$, $CaCO_3$), magnetite (Fe_3O_4), pyrrhotite $[(Fe,Ni)_{1-x}S]$, pentlandite $[(Fe,Ni)_9S_8]$, and most importantly, cubanite ($CuFe_2S_3$), which has not been identified in any other chondrite class. It is widely accepted that for the CI chondrites hydrothermal activity is responsible for the formation of these minerals and the phyllosilicates that comprise the bulk of the matrix (Herndon et al., 1975; Tomeoka and Buseck, 1988; Brearley, 2006), which constitutes 99% of the volume of these meteorites (Tomeoka and Buseck, 1988; Buseck and Hua, 1993; Weisberg et al., 2006). A notable difference between CI- and Stardust mineralogy is the lack of phyllosilicates in the Stardust collection. While observations of the debris plume from comet 9P/Tempel created by the Deep Impact experiment suggest the presence of phyllosilicates (Lisse et al., 2006), none have been reported from analyses of dust grains captured by the Stardust spacecraft from Wild 2. The lack of identified phyllosilicates in the Stardust samples may reflect diversity amongst comets or, if they were present on Wild 2, they may not have survived the capture process (Foster et al., 2008; Wozniakiewicz et al., 2010) or they may still be awaiting discovery in the Stardust collection (Zolensky et al., 2008a).

Stardust sulfides run the gamut between unmodified material to grains that appear to have been melted during capture into the aerogel (Zolensky et al., 2006). Comparisons between the hydrothermally altered sulfides from the CI chondrites and pristine sulfides from Wild 2 (i.e. those that have not been altered by capture into the aerogel), reveal similarities. Detailed characterization of these grains, which are sensitive to conditions and extent of alteration, aids in unravelling formation history. The key to any relationship between the Wild-2 and CI-chondrite sulfides may be the mineral cubanite. Prior to the Stardust mission, extraterrestrial cubanite had only been found in CI chondrites. It has been reported in Orgueil, Alais, and Ivuna (Macdougall and Kerridge, 1977; Kerridge et al., 1979; Bullock et al., 2005) and, now, in the Stardust collection. We directly compare the crystal structures and compositions of sulfides from both collections.

2. SAMPLES AND ANALYTICAL TECHNIQUES

Electron microprobe analyses (EMPA) of CI-chondrite samples were obtained using the Cameca SX-50 at the University of Arizona. Twelve thin sections of the CI chondrite Orgueil were prepared from samples provided by the Vatican Observatory. Each thin section was imaged and X-ray mapped for elements of interest. Sulfide grains were identified, analyzed for composition, and imaged. Analytical conditions were 15 kV and 40 nA, 20 s on peak and 20 s on background. Well-characterized standards were used and an internal PAP correction routine was used to correct for matrix effects. Detection limits (wt.%) are: $P = 0.02$, $S = 0.02$, $Fe = 0.09$, $Co = 0.06$, $Ni = 0.06$, $Cu = 0.14$, $Zn = 0.18$. Electron-transparent cross sections of an individual cubanite grain and a cubanite/pyrrhotite assemblage, from the Orgueil thin sections, were prepared at the Naval Research Laboratory (NRL) using an FEI Nova 600 focused ion beam (FIB) scanning electron microscope based on previously described methods (Zega et al., 2007).

For the Stardust samples we obtained transmission electron microscope (TEM) grids with ultramicrotome thin sections of terminal particles that had been prepared at Johnson Space Center (JSC) and the University of Washington. The microtome sections were of particles embedded in epoxy, typically ~70 nm thick. Most of the sections were relatively complete, but several exhibited chatter and loss of sample, so that some of the petrographic context was lost. Of the 31 microtome sections we investigated, nine contained sulfide melt droplets, and three, which we discuss in detail herein, contained crystalline sulfide grains [(C2054-5-26-1-16), (FC6-0-10-0-85), and (C2054-5-27-1-11)].

TEM analyses of CI-chondrite and Stardust sulfides were performed using the JEOL 2500SE 200 keV field-emission STEM and the JEOL 2000FX 200 keV STEM at JSC, and the 200 keV JEOL 2200FS at NRL. The JSC STEM is equipped with a Noran thin window energy-dispersive X-ray (EDX) spectrometer that enables rapid EDX mapping of samples. The resulting images contain a high count EDX spectrum in each pixel, enabling the determination of quantitative element abundances in addition to displaying the spatial distribution of major and minor elements. For the spectrum imaging, we rastered a 4 nm diameter incident probe with a dwell time of 50 μs/pixel to limit beam damage and element diffusion during the analysis. The size of the rastered area was typically 256 × 204 pixels at a magnification that was optimized to limit over- or under-sampling with the 4 nm probe. Successive image layers of the samples were acquired and combined in order to achieve <10% counting statistic error for major elements in each pixel. Spectrum images obtained on the NRL STEM, which is also equipped with a thin-window Noran EDX spectrometer, were done with 0.5–1.5 nm diameter incident probes, dwell times of 50 μs/pixel, and rastered areas of either 256 × 256 or 512 × 512 pixels. EDX spectra were quantified using Cliff–Lorimer thin film techniques with *k*-factors experimentally determined from well-characterized standards.

Selected-area electron-diffraction (SAED) patterns were acquired from grains of interest. SAED patterns from all instruments were measured based on calibrated camera constants, and comparisons with known structure types were used to identify phases. Where feasible, phase identification was based on both SAED patterns and EDX spectra. However, the small sizes of some grains rendered SAED patterns unobtainable, and in such cases, phase identification was based solely EDX spectra.

3. RESULTS

3.1. Stardust samples

3.1.1. Track 26 cubanite

A cubanite grain, fractured during the sample preparation, occurs near the exterior of a terminal particle from Stardust track 26 (C2054-5-26-1-16) (Fig. 1a and b) and is

distributed over an area of ~0.28 × 0.17 μm. The composition is consistent with stoichiometric $CuFe_2S_3$ embedded in aerogel (Table 1). SAED patterns from three orientations are consistent with low-temperature, orthorhombic cubanite (Fleet, 1971). The pattern from the [10–2] zone axis (Fig. 1c), along with Laue ring spacings in patterns from two other orientations are diagnostic of cubanite.

3.1.2. Track 10 sphalerite and pyrrhotite

TEM analyses reveal that Stardust track 10 contains a polycrystalline terminal particle measuring ~2.7 × 1.8 μm (FC6-0-10-0-85) (Fig. 2). It is predominantly Ni-free pyrrhotite, associated with a μm-sized grain of Ni-bearing pyrrhotite (~3.7 at.% Ni). The Ni-free and Ni-bearing pyrrhotite compositions (Table 1) fall within the stability field for 4C monoclinic pyrrhotite (Wang et al., 2006, and references therein). The assemblage also includes a μm-sized grain of Fe-rich sphalerite [(Fe,Zn)S], which contains roughly equivalent amounts of Fe and Zn, and minor Mn (<2 at.%). The sphalerite shows fine scale twinning on (1 1 1) and is separated from the Ni-rich pyrrhotite by the Ni-free pyrrhotite. Table 1 lists compositional data for these minerals. SAED patterns from the Ni-bearing pyrrhotite (zone axis [0 −4 1]) and the Ni-free pyrrhotite (zone axis [1 −1 0]) (Fig. 3) are consistent with 4C monoclinic pyrrhotite (Tokonami et al., 1972; Putnis, 1975; Posfai et al., 2000).

3.1.3. Track 27 pyrrhotite and pentlandite

Pyrrhotite and pentlandite occur ~1.2 μm apart in a track 27 terminal particle (C2054-5-27-1-11) (Fig. 4). We infer that prior to ultramicrotomy, the pyrrhotite and pentlandite grains were in direct contact; the grains were likely fragmented during sample preparation. The largest pentlandite fragment measures ~0.41 × 0.11 μm. The pyrrhotite fragments are more numerous and have an average size of ~0.30 × 0.10 μm. The pyrrhotite is essentially Ni-free, and falls compositionally within the stability field for 4C monoclinic pyrrhotite (Wang et al., 2006, and references therein). The pentlandite contains slightly more Ni than Fe (Table 1). SAED patterns taken from three compositionally equivalent pyrrhotite fragments and a pentlandite fragment are consistent with the 4C monoclinic pyrrhotite (zone axes: [1 −1 0], [11 24 −1] and [−1 18 −9]) and pentlandite structures (zone axis [0 1 −1]), respectively (Pearson and Buerger, 1956; Tokonami et al., 1972; Putnis, 1975; Posfai et al., 2000).

Table 1
Stardust sulfide compositions.

	Range or single value (at.%)	Mean (at.%)
Track 26 cubanite[*], $n = 1$		
Fe	35.0 ± 0.5	–
Cu	15.3 ± 0.7	–
S	49.7 ± 0.5	–
Track 27 pyrrhotite, $n = 5$		
Fe	45.0–46.7	45.8
Ni	0.0–0.2	0.2
S	53.0–55.0	54.1
Track 27 pentlandite, $n = 2$		
Fe	22.0–22.5	22.2
Ni	26.0–26.1	26.0
S	51.4–52.0	51.7
Track 10 Ni-free pyrrhotite, $n = 3$		
Fe	45.1–46.3	45.5
Ni	b.d.l.	–
S	53.7–54.9	54.5
Track 10 Ni-bearing pyrrhotite, $n = 1$		
Fe	42.7 ± 0.5	–
Ni	3.7 ± 0.8	–
S	53.6 ± 0.5	–
Track 10 sphalerite, $n = 2$		
Mn	1.1–1.2	1.2
Fe	21.9–24.3	23.1
Zn	21.9–24.6	23.2
S	52.3–52.7	52.5

[*] Si and O contributions from aerogel subtracted; n = # of grains analyzed; b.d.l. = below detection limits.

3.2. CI chondrite samples

In Orgueil, cubanite occurs either as individual grains or intimately associated with pyrrhotite. EMPA results (ranges and means) for 107 pyrrhotite grains and 19 cubanite grains (17 individual grains and 2 intergrown with pyrrhotite) are reported in Table 2. Ten of the pyrrhotite grains have domains with higher than average Ni-contents. TEM analyses were performed on FIB-prepared electron-

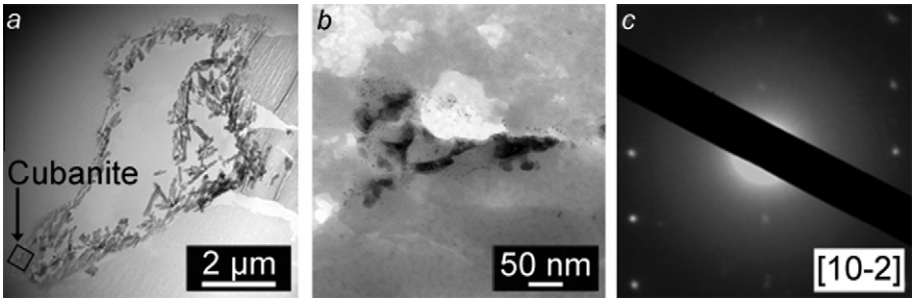

Fig. 1. (a) Bright field image (BFI) of a terminal particle from Stardust track 26 (C2054-5-26-1-16) with a cubanite grain located on the exterior. (b) Close-up BFI of a compositionally stoichiometric cubanite grain ($CuFe_2S_3$) (Table 1). (c) Selected area electron diffraction pattern from the [1 0 −2] zone axis, consistent with the low-temperature orthorhombic polymorph of $CuFe_2S_3$, which indicates that the grain has not been heated above 210 °C.

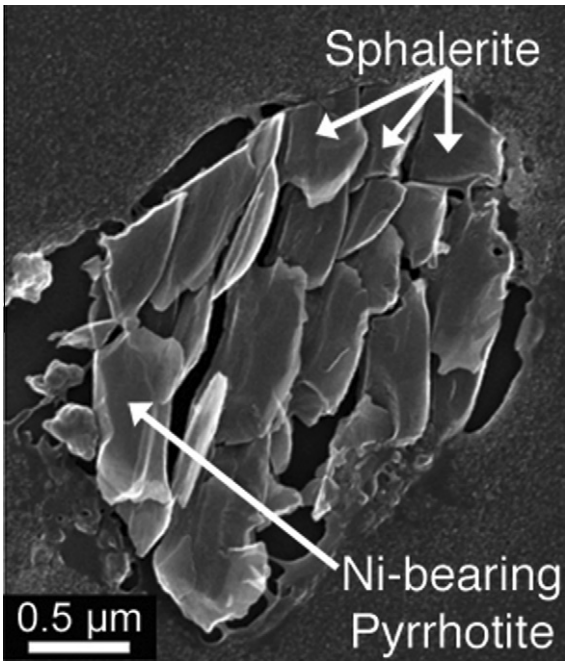

Fig. 2. High angle annular dark field image of Stardust track 10 pyrrhotite/sphalerite assemblage (FC6-0-10-0-85). The sphalerite and Ni-bearing pyrrhotite grains are indicated. The remainder of the particle is Ni-free pyrrhotite. The compositions of the pyrrhotites (Ni-bearing and Ni-free) (Table 1) fall within the 4C monoclinic pyrrhotite stability field.

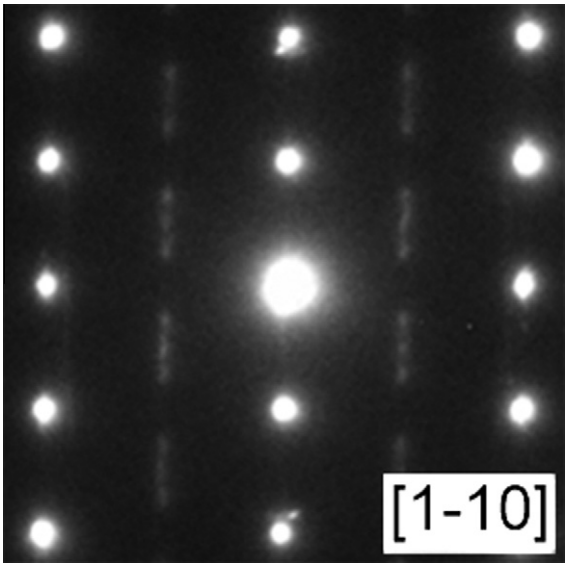

Fig. 3. Selected area electron diffraction (SAED) pattern from Stardust track 10 4C monoclinic pyrrhotite (zone axis [1 −1 0]). A pattern collected from Stardust track 27 4C monoclinic pyrrhotite is identical. This polymorph of pyrrhotite is not stable above ~250 °C.

transparent sections from an individual cubanite grain (Fig. 5) and an assemblage of cubanite overgrowing pyrrhotite (Fig. 6). Compositionally, TEM-EDX analyses agree, within error, with EMPA results for both the cubanite grain and the cubanite/pyrrhotite assemblage's main crystals (Table 3). The petrography and crystallography of the TEM-investigated sulfides are discussed below.

3.2.1. Individual cubanite grain

TEM analyses of the cubanite FIB section (~8.4 × 5.9 μm) reveal a single crystal crosscut by a vein (Fig. 5a). SAED patterns obtained in three orientations from the bulk cubanite (zone axes: [0 1 0], [0 1 −1], and [1 2 −1]), both above and below the vein, are consistent with the low-temperature orthorhombic form (Fleet, 1971). The composition of the grain is consistent with stoichiometric cubanite. In comparison, the vein consists of three amorphous layers (Fig. 5b). The outer layer contains Cu, Fe, and S, with higher Cu:S and lower Fe:S ratios than the adjacent cubanite. The interior layer contains an Fe-, Ni- and O-bearing material. A Ca-, S-, and O-bearing material occurs in the center of the amorphous region, although not throughout the entire vein.

3.2.2. Cubanite/pyrrhotite assemblage

The ~10.7 × 7.3 μm FIB section of this assemblage (Fig. 6) consists of four crystalline areas separated by a crosscutting vein: larger cubanite and pyrrhotite grains to the upper left and right, respectively, and smaller grains of pyrrhotite and a Cu–Fe sulfide located centrally towards the bottom of the section. The large cubanite grain is compositionally homogenous at the nm-scale and congruently oriented both above and below the vein. Measurements of cubanite SAED patterns from two orientations are consistent with the low-temperature orthorhombic polymorph (Fleet, 1971). The pattern from the [3 −1 0] zone axis (Fig. 7a) has faint reflections which echo the brighter ones in two directions and doublets in one direction, while the [2 −1 0] zone axis pattern has faint spots in one direction, but no doublets. The small Cu–Fe-sulfide grain that occurs between the pyrrhotite grains is depleted in Cu and S and enriched in Fe relative to the main cubanite crystal. Its SAED pattern (only obtained from one orientation) is consistent with cubanite ([3 −1 0] zone axis).

Measurements of the interplanar spacings and angles from SAED patterns of the large pyrrhotite grain are consistent with the 4C monoclinic structure, zone axis [−1 0 1]. The crystal is homogenous in composition and orientation. The smaller pyrrhotite grain is a twinned 4C monoclinic pyrrhotite crystal ([0 1 0] and [1 1 0] zone axes, Fig. 7b) (Tokonami et al., 1972; Putnis, 1975; Posfai et al., 2000) that is oriented differently from the main pyrrhotite grain, although it is within 1 at.% of the composition of the other pyrrhotite grain. And, like the Stardust pyrrhotites, the Orgueil pyrrhotite composition falls within the stability field for 4C monoclinic pyrrhotite (Wang et al., 2006, and references therein).

The vein material is similar to that described above. The vein cross-cutting the largest cubanite grain is free of Ca-bearing material, whereas that between the main cubanite and pyrrhotite crystals contains all three layers. In addition, Hg-sulfide grains are dispersed in the area between the small pyrrhotite grain and the small Cu–Fe-sulfide, as well as below the main cubanite grain.

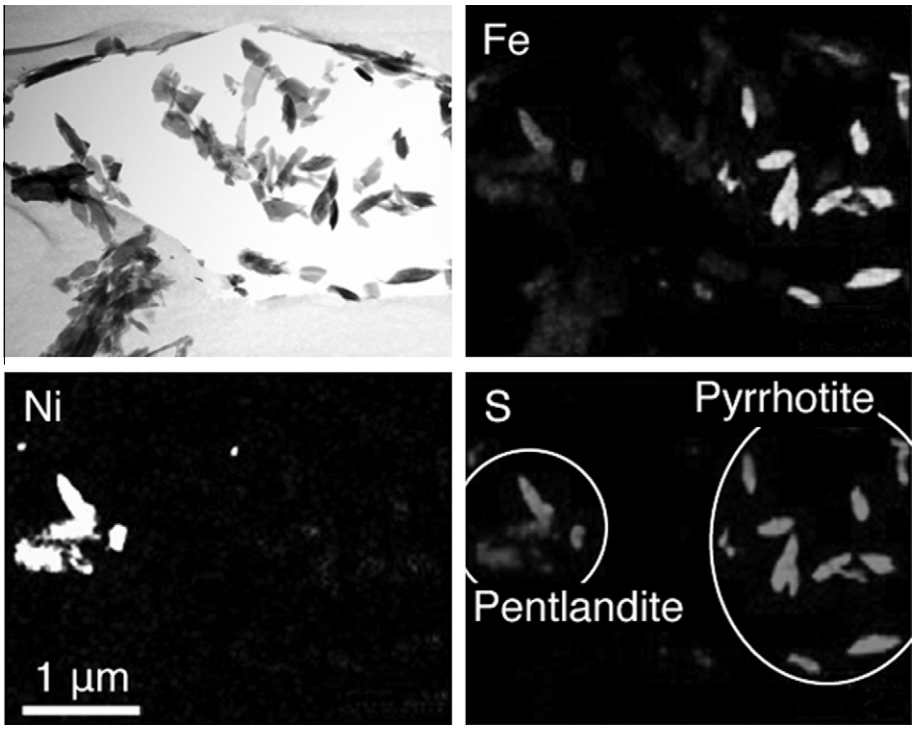

Fig. 4. Bright field image and X-ray maps of the Stardust track 27 terminal particle (C2054-5-27-1-11). The pyrrhotite grains are compositionally equivalent (Table 1), and fall within the 4C monoclinic pyrrhotite stability field. The pentlandite grains are compositionally equivalent to one another.

Table 2
Orgueil sulfide compositions.

	Range or single value (at.%)	Mean (at.%)
Cubanite, $n = 19$		
Fe	32.8–33.9	33.4
Cu	15.8–16.8	16.3
S	49.4–51.0	50.3
Pyrrhotite, $n = 107$		
Fe	44.2–46.7	45.8
Co	b.d.l.	–
Ni	0.0–1.1	0.8
Cu	0.0–0.1	0.0
S	52.6–54.9	53.4
Ni-rich domains within pyrrhotite grains, $n = 10$		
Fe	24.0–45.2	37.4
Co	0.0–0.9	0.4
Ni	1.4–27.3	10.9
Cu	0.0–0.1	0.0
S	47.5–53.5	51.5

n = # of grains analyzed; b.d.l. = below detection limits.

4. DISCUSSION

EMPA and TEM analyses reveal similarities between the Wild-2 sulfides and those from the hydrothermally altered CI-chondrite Orgueil. Distinctive structural characteristics (e.g. irreversible phase transitions, vacancy ordering) allow for the placement of constraints on formation conditions. In turn, these constraints have implications for when and where formation and alteration occurred. They speak to both radial mixing of material forming at lower temperatures than CAIs and to the possibility for hydrothermal alteration on a cometary body.

4.1. Constraints from structure, composition, and comparative mineralogy

4.1.1. Wild-2 and CI-chondrite cubanite

Cubanite ($CuFe_2S_3$) has been found in terrestrial ore deposits, CI chondrites, and in the Stardust collection; it has not been reported in other chondritic meteorites. There are two polymorphs of $CuFe_2S_3$: cubanite, the low-temperature orthorhombic form and isocubanite, the high-temperature cubic form. Cubanite undergoes an irreversible phase transition to isocubanite at 210 °C (Fleet, 1971; Cabri, 1973; Szymanski, 1974; Caye et al., 1988). Upon cooling below 210 °C, isocubanite does not revert to cubanite, but rather exsolves or breaks down to chalcopyrite ($CuFeS_2$) and pyrrhotite (Cabri, 1973; Putnis, 1977; Kaneda et al., 1978; Pruseth et al., 1999). As detailed above, SAED patterns from the Stardust track 26 $CuFe_2S_3$ are consistent with low-temperature, orthorhombic cubanite. The irreversibility of the structural transformation establishes that the Wild-2 cubanite must have formed at low temperature, did not experience temperatures above 210 °C prior to or during its residence on Wild 2, and it was not significantly heated during capture into aerogel.

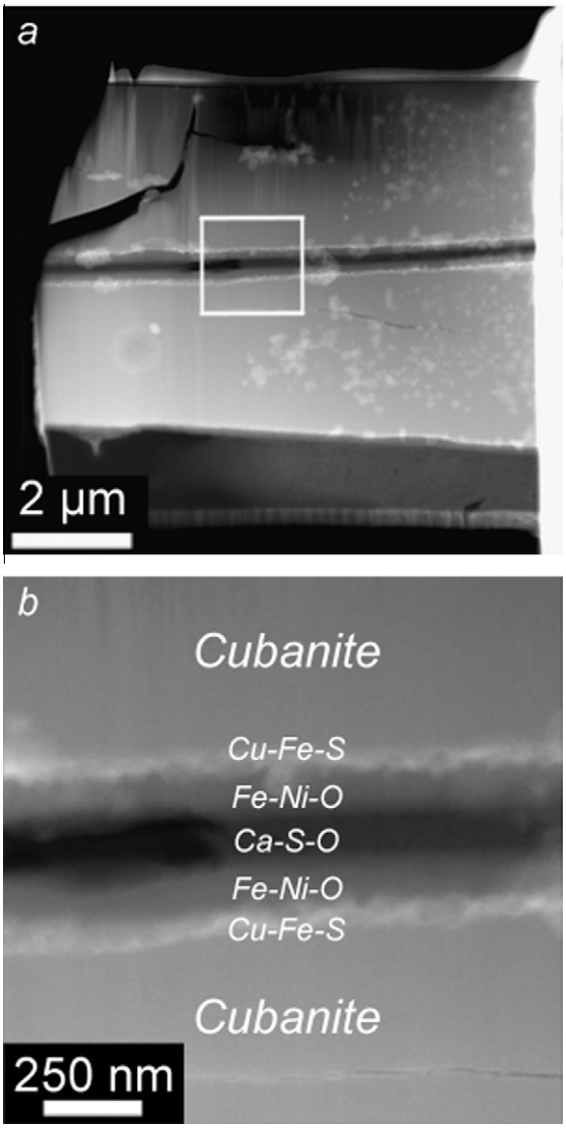

Fig. 5. (a) High angle annular dark field (HAADF) image of the FIB-prepared thin section of a single crystal of Orgueil cubanite. (b) Close-up HAADF image of the cross-cutting vein which postdates the formation of the cubanite. The Cu–Fe–S vein layer is depleted in Fe and enriched in Cu relative to the cubanite. Material in all vein layers is amorphous.

4.1.2. Wild-2 and CI-chondrite pyrrhotite

The metal deficient Fe sulfide pyrrhotite, like cubanite, exists in more than one structural form (e.g. monoclinic or hexagonal), and ordering of the Fe vacancies (i.e. stacking of layers) can also vary (e.g. Dodony and Posfai, 1990; Posfai and Dodony, 1990; Posfai and Buseck, 1997; Makovicky, 2006). While there is not an irreversible phase transition between the different polytypes and polymorphs, there are compositional and thermal regions of stability for each (Wang et al., 2006, and references therein). As discussed above, the presence of cubanite evidences temperatures below 210 °C. Likewise, the presence of 4C monoclinic pyrrhotite, on its own, is indicative of low temperatures; it is not stable above ~250 °C (Wang et al., 2006, and references therein). The 4C monoclinic structure is better able to stabilize Fe vacancies than the other pyrrhotite polymorphs (Fleet, 1968; Tokonami et al., 1972; Putnis, 1975). Experimental work by Hall and Yund (1966) showed that as temperatures decrease, monoclinic pyrrhotite becomes more Fe deficient; they attained an Fe content for pyrrhotite of 46.3% at 70 °C (albeit in the presence of pyrite) similar to the total metal content (Fe + Ni) of our Orgueil and Stardust pyrrhotites (Tables 1 and 2). Lastly, monoclinic pyrrhotite has been synthesized under low-temperature aqueous conditions (Sugaki and Shima, 1965) that do not exclude the formation of cubanite.

While the cubanite and pyrrhotite crystal structures provide temperature constraints, the petrographic context of the combination of pyrrhotite and cubanite in the CI-chondrites provides more detailed information about potential formation mechanisms. Petrologic evidence suggests that the cubanite in Orgueil formed after the pyrrhotite (e.g. Fig 6a); examples of cubanite overgrowths on pyrrhotite have also been reported in the CI chondrite Alais (Bullock et al., 2005). Pyrrhotite and cubanite do not form a stable assemblage on the 200 °C Cu–Fe–S ternary diagram (Yund and Kullerud, 1966; Kullerud et al., 1969). They do, however, have a tie line between them in an extrapolated 25 °C Cu–Fe–S ternary (Vaughan and Craig, 1997) (Fig. 8). The combination of pyrrhotite and cubanite indicates lower temperatures than either mineral alone. The structural and compositional data for these sulfides are in line with the petrologic evidence that cubanite formed at a later stage than pyrrhotite by precipitating from an aqueous fluid as the parent body cooled (Bullock et al., 2005).

While pyrrhotite has not been identified in conjunction with cubanite in the Stardust collection, we have identified it in multiple tracks. The track 10 and 27 pyrrhotites' structures (4C monoclinic) not only imply temperatures below ~250 °C, but also indicate that the grain was not heated significantly during capture into the aerogel. Quenching of monoclinic pyrrhotite, from temperatures of 500 °C, produces hexagonal pyrrhotite (O'Reilly et al., 2000), rather than the more ordered monoclinic structure, which maximizes the distances between Fe vacancies (Fleet, 1968; Tokonami et al., 1972; Putnis, 1975). Cooling rates of ~10 °C/min would be required to retain the monoclinic structure (O'Reilly et al., 2000). Additionally, the transition from hexagonal to monoclinic pyrrhotite requires prolonged annealing at 150–200 °C (Yund and Hall, 1969; O'Reilly et al., 2000). So, as in the case of the cubanite, the 4C pyrrhotite found in these Stardust samples is pristine cometary material that has not been altered by the capture process.

4.1.3. Wild-2 and CI-chondrite pentlandite

The combination of pyrrhotite and pentlandite has been observed in both the CI-chondrite and Stardust collections. The Ni contents of the track 27 pentlandite and pyrrhotite grains fall within the average values reported for CI chondrites (Bullock et al., 2005), providing another link between CI-chondrite and Stardust minerals. Pentlandite and pyrrhotite in the CI-chondrite collection often occur in direct contact (Kerridge et al., 1979; Bullock et al., 2005), and the track 27 pyrrhotite and pentlandite were likely in phys-

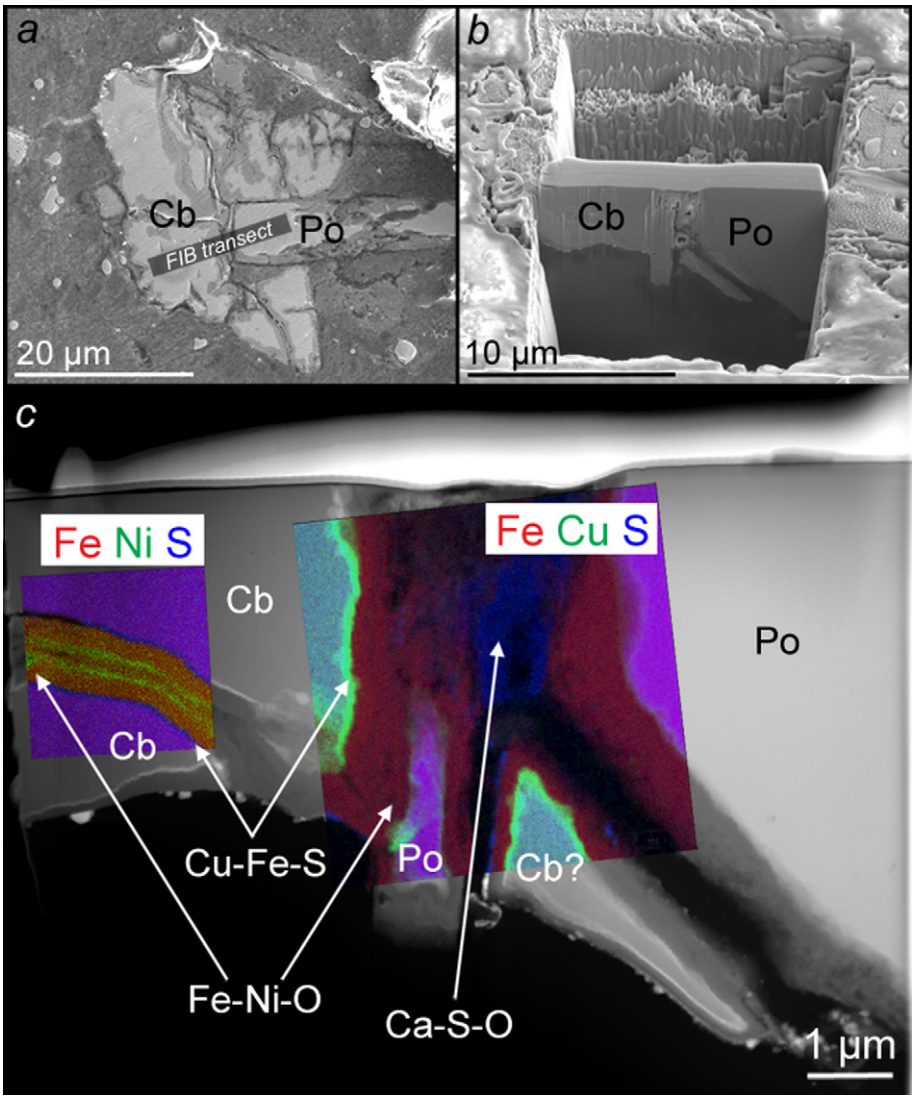

Fig. 6. (a) Back scattered electron image of an Orgueil cubanite grain overgrowing pyrrhotite. (b) Secondary electron image taken during the FIB preparation of electron transparent cross-section. (c) High angle annular dark field image of the FIB-prepared thin section of the cubanite/pyrrhotite interface with X-ray maps superimposed. The main cubanite crystals (Cb) are stoichiometric cubanite, $CuFe_2S_3$. The pyrrhotite (Po) grain compositions fall within the 4C monoclinic pyrrhotite stability field. The "Cb?" is depleted in Cu and enriched in Fe relative to $CuFe_2S_3$, but crystallographically indexes to cubanite in one orientation. The vein material is amorphous. Note: The dark space at the bottom of 5c is epoxy.

Table 3
TEM-investigated CI-chondrite sulfide compositions.

	at.% ± 2σ
Individual cubanite grain	
Fe	33.2 ± 0.4
Cu	16.3 ± 0.2
S	50.5 ± 0.4
Assemblage cubanite grain	
Fe	33.1 ± 0.4
Cu	16.4 ± 0.2
S	50.5 ± 0.6
Assemblage pyrrhotite grain	
Fe	45.4 ± 0.3
Ni	1.0 ± 0.1
S	53.6 ± 0.3

ical contact prior to capture into the aerogel but were disrupted during the sample preparation procedure. By itself, pentlandite is a sign of low-temperature aqueous alteration (Zolensky and Thomas, 1995; Bullock et al., 2005; Zolensky et al., 2008a), but the combination of pentlandite and pyrrhotite yields more detailed constraints than either phase alone. Their association is significant because the 100–135 °C Fe–Ni–S phase diagram (Fig. 9) has tie lines between the sulfides that are not present on the 250 °C phase diagram (Naldrett, 1989), indicating a low equilibration temperature (Bullock et al., 2005).

4.1.4. Wild-2 and CI-chondrite sphalerite

The track 10 assemblage includes a μm-sized grain of Fe-rich sphalerite with minor Mn in direct contact with pyrrhotite. Sphalerite grains with minor Mn have also been

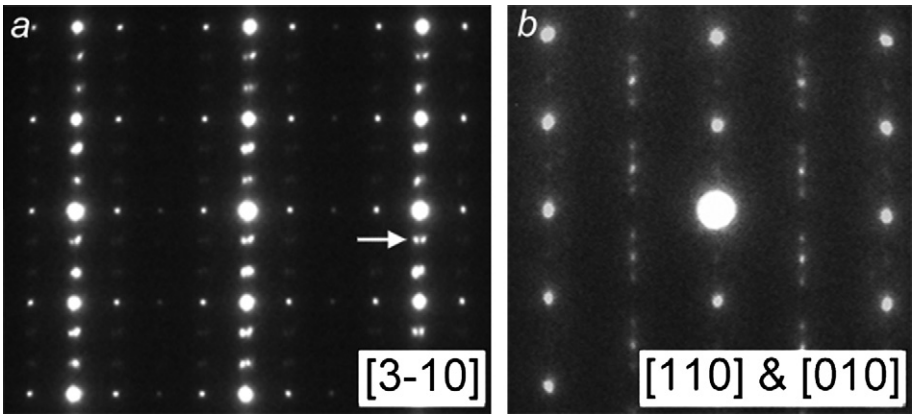

Fig. 7. (a) A cubanite selected area electron diffraction (SAED) pattern from the Orgueil cubanite/pyrrhotite assemblage. Bright spots are consistent with the [3 −1 0] zone axis of cubanite. The orthorhombic crystal structure indicates a maximum temperature of 210 °C. Fainter spots (e.g. vertical columns between brighter columns) and doublets (e.g. spots indicated by the arrow) in the diffraction pattern are suggestive of structural variations due to vacancy ordering or a cation superlattice. (b) SAED pattern from the Orgueil 4C monoclinic pyrrhotite containing twinned [1 1 0] and [0 1 0] zone axes. This polymorph of pyrrhotite is not stable above ~250 °C.

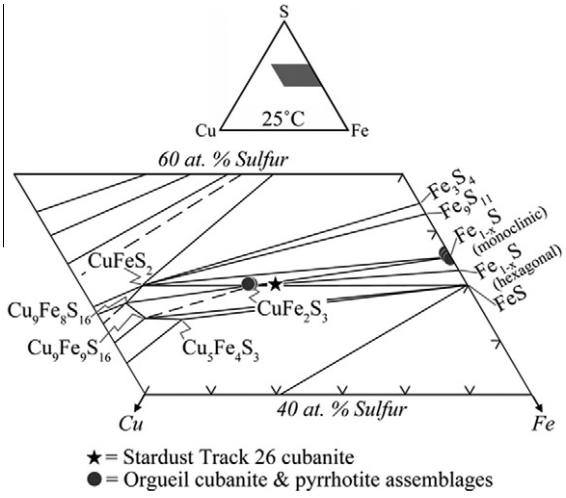

Fig. 8. 25 °C Cu–Fe–S ternary diagram (after Vaughan and Craig, 1997) with Stardust track 26 cubanite and CI-chondrite cubanite/pyrrhotite assemblage compositions plotted. The tie line that appears between cubanite and pyrrhotite in this ternary diagram is not present in the 200 °C ternary, indicating that the combination of cubanite and pyrrhotite form a stable assemblage at low temperatures.

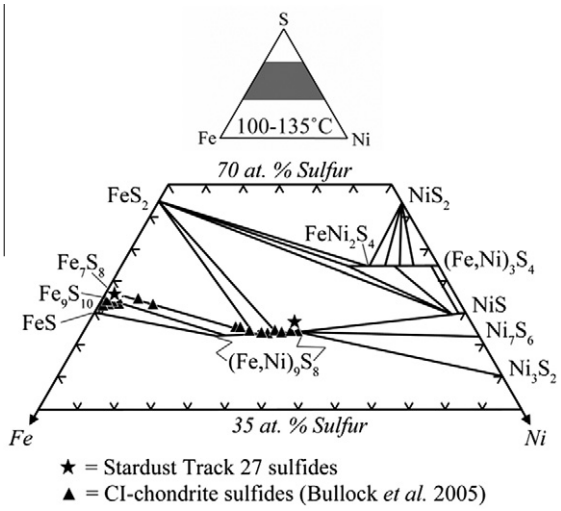

Fig. 9. 100–135 °C Fe–Ni–S ternary diagram (after Naldrett, 1989) with Stardust track 27 pyrrhotite and pentlandite and CI-chondrite sulfide compositions plotted. Tie lines between pyrrhotite and pentlandite are not present in the 250 °C Fe–Ni–S ternary diagram, indicating this assemblage has a low equilibration temperature.

reported in the interplanetary dust particle (IDP) Attilla (Christoffersen and Buseck,1986), although the IDP's sphalerite has a much lower Fe content than the track 10 sphalerite. Attilla also contains multiple pyrrhotite grains with an order of magnitude less Ni than the Ni-rich pyrrhotite grain in the track 10 assemblage. The Stardust pyrrhotite/sphalerite assemblage does not have an exact analogue in the aqueously altered CI-chondrite suite. However, sphalerite is commonly found in terrestrial hydrothermal ore deposits with pyrrhotite and/or pyrite (Kullerud et al., 1969), so it is not surprising that some CI-chondrite pyrrhotites contain Zn. The elemental abundance of Zn in CI chondrites is >300 ppm (Anders and Grevesse, 1989). Trace element analyses of CI-chondrite pyrrhotites reveal a large degree of variability in Zn content: from 0 to 181 ppm (Greshake et al., 1997). Preliminary laser-ablation inductively coupled mass spectrometry measurements suggest the possibility of sphalerite inclusions within Orgueil pyrrhotite grains. Work is ongoing to determine the relationship between these phases in CI chondrites.

4.1.5. CI-chondrite minor phases

Hydrothermal activity is responsible for the minor phases in the Orgueil TEM sections: Hg-sulfide and the vein material, which postdates the formation of the sulfides. The Fe depletion in the outer layer of the vein is consistent with Fe being preferentially removed (vis-à-vis Cu) from Cu–Fe-sulfides during oxidation or weathering (Vaughan and Craig, 1997). The Ca-, S-, and O-bearing material is

presumably a sulfate which could have formed in situ on the parent body or may be a product of terrestrial weathering (Gounelle and Zolensky, 2001; Airieau et al., 2005). Mercury-sulfide in CM chondrites is the product of low temperature aqueous alteration on the parent body (Lauretta et al., 1999); its presence in Orgueil is indicative of an analogous process on the CI-parent body. (The small size of the Orgueil HgS grains precluded phase identification via SAED.) Modeling of hydrous asteroids (CM- and CI-like) predicts alteration temperatures of 50–150 °C (Zolensky et al., 1989) and data from oxygen isotopes suggest an alteration temperature of ~150 °C (Clayton and Mayeda, 1999). Thus, the predicted low-temperature alteration for the CI-chondrite parent body is supported by the presence of mercury sulfide, 4C monoclinic pyrrhotite, and cubanite.

4.1.6. Alteration of sulfides during capture into the aerogel

Sub-micron Fe–Ni–S melt droplets, many of which consist of Fe–Ni cores surrounded by sulfide rims, and sulfide melt on the edges of particles, have been modified by capture into the aerogel, and are common in the Stardust collection. We have identified them in nine microtome sections: Track 26 Ada, C2017-2-99-1-7, C2017-2-99-2-8, C2017-2-100-3-12, C2054-5-27-1-1, C2063-1-154-1-10, C2081-1-108-2-9, C2081-1-108-20-3, and C2092-7-81-2-2. They have also been reported by: Brownlee et al., 2006; Keller et al., 2006; Zolensky et al., 2006; Ishii et al., 2008; Leroux et al., 2008; Nakamura et al., 2008; Rietmeijer et al., 2008; Tomeoka et al., 2008; Leroux et al., 2009; Stodolna et al., 2009; Velbel and Harvey, 2009. In contrast, and as mentioned above, the sulfides we report on here were not significantly modified during capture. Like the track 57 sulfide grain, investigated by Brownlee et al. (2006), our track 27 pyrrhotite and track 10 cubanite grains were part of larger mineral conglomerates, which may have protected the sulfides from being melted during capture. Additionally, larger sulfide grains may also have been spared from significant modification. Similar to the track 36 crystalline sulfide reported on by Zolensky et al., 2008a, our unmodified track 10 pyrrhotite, while not part of a conglomerate, is relatively larger than the track 26 and 27 sulfides.

4.1.7. Comparison to IDPs and AMMS

Comparison to pyrrhotites found in hydrated IDPs strengthens the case for Wild-2 sulfide formation by aqueous processing. A broad survey of sulfides in IDPs shows that pyrrhotites in anhydrous IDPs typically contain <2 at.% Ni while those in hydrated IDPs can contain up to ~15 at.% Ni (Zolensky and Thomas, 1995). This observation is supported by other studies of sulfides in individual IDPs (Tomeoka and Buseck, 1984; Christoffersen and Buseck, 1986; Dai and Bradley, 2001; Rietmeijer, 2004). However, Dai and Bradley (2001) report pyrrhotite with >2 at.% Ni among the anhydrous IDP population, although the Ni-content of most of the hexagonal pyrrhotite grains that they analyzed falls well below 2 at.%. In general, Ni-bearing pyrrhotite grains appear to be common in hydrated IDPs and rare in anhydrous IDPs.

Pentlandite grains in IDPs also correlate with the hydration state of their host particle. In general, pentlandite is found almost exclusively in hydrated IDPs (Tomeoka and Buseck, 1984; Zolensky and Thomas, 1995; Dai and Bradley 2001; Rietmeijer, 2004). Like our track 27 pentlandite, the Ni:Fe ratio is >1 for some hydrous IDP pentlandites (Tomeoka and Buseck, 1984; Zolensky and Thomas, 1995). The comparison between pentlandite in the Stardust collection and those in IDPs provides further support for our aqueous formation mechanism hypothesis.

Despite chemical similarities between the IDP and Stardust sulfides, the populations are crystallographically distinct. The track 10 and 27 pyrrhotites have the same 4C monoclinic structure as CI chondrite pyrrhotites. In contrast, the reported crystal structures of the IDP pyrrhotites are hexagonal (Tomeoka and Buseck, 1984; Christoffersen and Buseck, 1986; Dai and Bradley, 2001) and 'spinel-like' cubic (Dai and Bradley, 2001). The hexagonal structure may be the result of secondary heating processes (Dai and Bradley, 2001; Bradley, 2010) that occur during atmospheric entry of the IDPs (Brownlee, 1978). As suggested by Bradley (2010), the differing crystal structures of chondritic and IDP pyrrhotites indicate different formation environments. We suggest monoclinic Stardust and CI-chondrite pyrrhotites formed in an environment distinct from that of the IDP sulfides.

Troilite, pyrrhotite, and pentlandite occur in the Antarctic micrometeorite (AMM) collection (Engrand et al., 2007; Dobrică et al., 2009). These sulfides, which may partially derive from cometary sources (Liou and Zook, 1996), span a wide range of Ni-concentrations (Engrand et al., 2007; Dobrică et al., 2009). However, most Fe–Ni-sulfides in these samples contain <3 at.% Ni (Dobrică et al., 2009). The AMM pentlandite occurs in partially melted grains, suggesting alteration during a flash-heating event associated with atmospheric entry (Dobrică et al., 2009). A direct comparison between AMM and Stardust pyrrhotite crystal structures would be useful in delineating the relationship between the 2 populations.

4.2. Implications for solar system history

The combination of compositional and structural similarities between the track 10 and 27 pyrrhotites and CI-chondrite pyrrhotite is suggestive of hydrous processing for both populations. Overall, the CI-chondrite and Stardust sulfide suites are very similar: cubanite, 4C monoclinic pyrrhotite, pentlandite. The similarities are not only in composition and mineral associations, but also in structural detail. These similarities suggest equivalent formation mechanisms and conditions. The polymorphs and polytypes of cubanite and pyrrhotite are consistent with low-temperature, aqueous processing, as is the presence of the high-Ni phases (pentlandite and Ni-bearing pyrrhotite).

The most robust constraint from the mineral characterizations is that neither the cubanite in the Stardust collection nor that in the CI-chondrite collection has seen temperatures above 210 °C. The other sulfide associations suggest aqueous processing at significantly lower temperatures. If the Stardust sulfides formed via the same aqueous mechanisms as they did on the CI-chondrite parent body, they represent remnants of aqueous alteration on a come-

tary body. Where that alteration took place cannot be determined from the Stardust collection, since there is no petrologic context for the individual minerals. There are a number of possible pathways that culminate with low-temperature sulfides on comet Wild 2, some more probable than others. We focus on cubanite as we explore three possible scenarios below.

The first option is the formation of cubanite via nebular condensation or sulfidation of nebular condensates, followed by incorporation onto a parent body. Metal alloys that formed in the early solar system play host to many siderophile elements, including Ni and Cu (Lodders, 2003), which can partition into a sulfide phase during nebular corrosion. Troilite (FeS) can form quickly via corrosion of Fe alloy by H_2S gas in a nebular environment (Lauretta et al., 1996a,b, 1997, 1998; Lauretta, 2005; Pasek et al., 2005). However, it is unlikely that cubanite formed via corrosion of a Cu-bearing Fe alloy. First, neither cubanite nor isocubanite occur in any primitive type-3 chondrites, which are most likely to retain nebular signatures. Second, cubanite's formation below 210 °C suggests that its reaction kinetics would be too slow under nebular conditions.

The second and third alternatives involve the formation of cubanite via aqueous alteration on a parent body. The main precursor for the CI-chondrite sulfides is troilite (FeS) (Bullock et al., 2005). Once FeS is incorporated onto the CI-chondrite parent body, it is oxidized via aqueous activity to magnetite, pyrrhotite, pentlandite, and cubanite (e.g. Herndon et al., 1975; Bullock et al., 2005). Stardust cubanite could have formed in situ on Wild 2 via a similar process, or it could be a remnant from a CI-chondrite-like parent body that was delivered out to the comet-forming region. Both possibilities are explored below.

If the Stardust cubanite formed on a CI-chondrite-like parent body, and the parent body was subsequently disrupted, the cubanite could have been delivered to the comet-forming region as part of a larger CI-conglomerate. Delivery of material to the comet-forming region requires large-scale mixing in the early nebula, and any mechanism invoked to radially transport the cubanite must keep it below 210 °C. The Stardust collection contains fragments of CAI- and chondrule-like material (e.g. Zolensky et al., 2006), high temperature nebular components that formed over timescales of tens of thousands (MacPherson et al., 2010) to ~100,000 years and 4 million years (Apai and Lauretta, 2010), respectively. Radial migration models demonstrate that these high-temperature solids can be moved beyond 20AU on timescales of ~100,000 years (e.g. Bockelee-Morvan et al., 2002; Ciesla, 2009).

A limiting factor in the timing of the migration is the formation of Jupiter and the clearing of gas from the nebula. Once Jupiter formed, mid-plane migration of small particles out to the comet-forming region was no longer possible (Ciesla, 2009). Estimates for the timescale of Jupiter's formation are on the order of several million years (e.g. Hersant et al., 2001; Hubickyj et al., 2005; Lissauer et al., 2009). Using ^{53}Mn data, it has been shown that aqueous alteration on the Orgueil parent body started ~3 Ma after solar system formation (anchored to the angrite LEW 86010) and continued for several million years (Hoppe et al., 2008). The timing of this alteration is either cotemporal or postdates the estimates for the timing of Jupiter's formation (e.g. Lissauer et al., 2009). Thus, the turbulent processes invoked to radially transport the CAIs and other high-temperature assemblages (e.g. Bockelee-Morvan et al., 2002; Ciesla, 2009) cannot be used to transport cubanite and the other low temperature sulfides from a CI-chondrite parent body to the comet-forming region. However, sulfide precursor material (FeS) could be moved out to the comet-forming region well within the time-scale mandated by Jupiter's formation. Modeling of nebular troilite formation predicts that it starts forming ~500,000 years after solar system formation, between 1 and 1.6 AU at 690 K, and that smaller metal grains could be sulfidized to troilite at distances up to at least 6 AU (Pasek et al., 2005). The same turbulent processes that move the CAIs and chondrules outward could also be responsible for moving FeS out to the comet-forming region. Any troilite discovered in the Wild-2 collection is likely to be nebular in origin.

Once at the comet, pockets of liquid with fluid conditions (e.g. Eh, pH, T, S-fugacity) analogous to those on the CI-chondrite parent body could convert the troilite and remnant metal to the suite of sulfides we see in Stardust. Fink et al. (1999) observed elevated NH_2 in Wild 2's coma, allowing for the possibility of a water-ammonia brine. The ammonia-water system has a eutectic temperature of −100 °C (Lewis, 2004), requiring less heat input for a liquid phase than a pure water system. Pockets of liquid could form on the comet due to heating from low-velocity collisions (McSween and Weissman, 1989; de Bergh et al., 2004; Lisse et al., 2006) which could occur throughout the comet's lifetime or short-lived radionuclides (if comets formed rapidly enough to accrete chondritic levels of ^{26}Al) (McSween and Weissman, 1989), which would be limited to the comet's early lifetime. Liquid, whether pure water or ammonia-water would not have to be long-lived, because aqueous formation of sulfides is rapid, even at low temperatures (McSween and Weissman, 1989). The advantage of this third scenario is that the radial transport mechanisms are not hindered by the low-temperatures (<210 °C) mandated by cubanite, nor are they precluded by the formation of Jupiter. If aqueous alteration occurred on the comet, then models of comet formation and processing need to account for the heat source, which could help constrain availability of short-lived radionuclides in the outer nebula.

Regardless of the mechanisms invoked to mix material in the nebula, the fate of minerals forming at temperatures lower than those at which CAIs and chondrules form must be considered. The mineralogy of comet Wild 2 requires radial mixing of materials, from the high temperature regime of CAI-like materials to the temperatures of Fe-sulfide formation or the low-temperature stability limits of the observed sulfide assemblages. In either case it is clear that comets preserve evidence of aqueous processes in the early Solar System. Unravelling the location and extent of this alteration requires samples that preserve the petrographic context, such as those obtained by a comet surface sample return mission.

5. CONCLUSION

We investigated sulfides from the Stardust and CI-chondrite collections via TEM and EMPA; in particular, Stardust samples: C2054-5-26-1-16 (cubanite), C2054-5-27-1-11 (4C monoclinic pyrrhotite and pentlandite), and FC6-0-10-0-85 (sphalerite, Ni-bearing and Ni-free 4C monoclinic pyrrhotite), as well as a cubanite grain and a cubanite/4C monoclinic pyrrhotite assemblage from the CI chondrite Orgueil. These sulfides and their associations are similar across the sample sets. The compositions, crystal structures, and phase relationships of these grains reveal that they formed via low-temperature aqueous processes.

To date, sulfides represent the strongest evidence of aqueous processes on Wild 2. The constraints afforded by the sulfides help to unravel the pathways by which they came to reside on Wild 2. We suggest that the most likely scenario resulting in the presence of cubanite on Wild 2 starts with radial mixing of nebular troilite out to the comet-forming region. After incorporation onto the cometary body, heating from low-velocity collisions or short-lived radionuclides provides energy to form pockets of liquid in which troilite and associated metals are converted into the suite of sulfides we see in the Stardust collection. If alternatively, the Wild-2 sulfides formed in the inner solar system and were subsequently delivered to the comet-forming region, the cubanite requires transport mechanism that is not hindered by the formation of Jupiter, and operates at temperatures below the upper stability limit of cubanite.

The in-depth characterization of Stardust sulfide grains and their CI-chondrite analogs furnishes constraints not only on the history of these particular grains, but also on large-scale processes that occurred in the early nebula, including heat sources and aqueous alteration on a cometary body, as well as mechanisms and extent of radial mixing of material. Taken together with information afforded by other minerals (e.g. CAIs) we can begin to assemble a more complete picture of early Solar System evolution.

ACKNOWLEDGEMENTS

Special thanks to G. Consolmagno and the Vatican Observatory for providing samples of Orgueil. We thank D. Brownlee, D. Joswiak and G. Matrajt, at the University of Washington; K. Nakamura-Messenger for assistance in Stardust sample selection; and CAPTEM for providing Stardust samples; Emma Bullock, Hughes Leroux, and an anonymous referee for constructive reviews; and Associate Editor, Sara Russell, for helpful comments. This work was supported by NASA grants: NNX08AW48H (ELB), NNH08AH58I (Rhonda Stroud PI, TJZ Co-I), 06-SSAP06-0026 (Scott Messenger PI, LPK Co-I), and NNX09AC60G (DSL PI).

REFERENCES

Airieau S. A., Farquhar J., Thiemens M. H., Leshin L. A., Bao H. and Young E. (2005) Planetesimal sulfate and aqueous alteration in CM and CI carbonaceous chondrites. *Geochim. Cosmochim. Acta* **69**, 4166–4171.

Anders E. and Grevesse N. (1989) Abundances of the elements – meteoritic and solar. *Geochim. Cosmochim. Acta* **53**, 197–214.

Apai D. and Lauretta D. S. (2010) Planet formation and protoplanetary dust. In *Protoplanetary Dust: Astrophysical and Cosmochemical Perspectives* (eds. D. Apai and D. S. Lauretta). Cambridge University Press, Cambridge. pp. 1–26.

Bockelee-Morvan D., Gautier D., Hersant F., Hure J.-M. and Robert F. (2002) Turbulent radial mixing in the solar nebula as the sources of crystalline silicates in comets. *Astron. Astrophys.* **384**, 1107–1118.

Bradley J. (2010) The astromineralogy of interplanetary dust particles. In *Astromineralogy, Lecture Notes in Physics, Vol. 815* (ed. T. Henning). Springer-Verlag, Berlin. pp. 259–276.

Brearley A. (2006) The action of water. In *Meteorites and the Early Solar System II* (eds. D. S. Lauretta and H. Y. McSween). University of Arizona Press, Tucson. pp. 587–624.

Bridges J. C., Burchell M. J., Changela C. C., Foster N. J., Creighton J. A., Carpenter J. D., Gurman S. J., Franchi I. A. and Busemann H. (2010) Iron oxides in comet 81P/Wild 2. *Meteorit. Planet. Sci.* **45**, 55–72.

Brownlee D. (1978) Interplanetary dust: possible implications for comets and presolar interstellar grains. In *Protostars and Planets* (ed. T. Gehrels). University of Arizona Press, Tucson, pp. 134–150.

Brownlee D., Tsou P., Aleon J. and 181 Others (2006) Research article – comet 81P/Wild 2 under a microscope. *Science* **314**, 1711–1716.

Bullock E. S., Gounelle M., Lauretta D. S., Grady M. M. and Russell S. S. (2005) Mineralogy and texture of Fe–Ni sulfides in CI1 chondrites: clues to the extent of aqueous alteration on the CI1 parent body. *Geochim. Cosmochim. Acta* **69**, 2687–2700.

Burchell M. J. and Kearsley A. (2009) Short-period Jupiter family comets after Stardust. *Planet. Space Sci.* **57**, 1146–1161.

Buseck P. R. and Hua X. (1993) Matrices of carbonaceous chondrite meteorites. *Annu. Rev. Earth Planet. Sci.* **21**, 255–305.

Cabri L. J. (1973) On the transformation of cubanite. *Can. Mineral.* **12**, 33–38.

Caye R., Cervelle B., Cesbron F., Oudin E., Picot P. and Pillard F. (1988) Isocubanite, a new definition of the cubic polymorph of cubanite $CuFe_2S_3$. *Mineral. Mag.* **52**, 509–514.

Christoffersen R. and Buseck P. R. (1986) Mineralogy of interplanetary dust particles from the "olivine" infrared class. *Earth Planet. Sci. Lett.* **78**, 53–66.

Ciesla F. J. (2009) Two-dimensional transport of solids in viscous protoplanetary disks. *Icarus* **200**, 655–671.

Clayton R. N. and Mayeda T. K. (1999) Oxygen isotope studies of carbonaceous chondrites. *Geochim. Cosmochim. Acta* **63**, 2089–2104.

Dai Z. R. and Bradley J. (2001) Iron–nickel sulfides in anhydrous interplanetary dust particles. *Geochim. Cosmochim. Acta* **65**, 3601–3612.

de Bergh C., Boehnhardt H., Barucci M. A., Lazzarin M., Fornasier S., Romon-Martin J., Tozzi G. P., Doressoundiram A. and Dotto E. (2004) Aqueous altered silicates at the surface of two Plutinos? *Astron. Astrophys.* **416**, 791–798.

Dobrică E., Engrand C., Duprat J., Gounelle M., Leroux H., Quirico E. and Rouzaud J.-N. (2009) Connection between micrometeorites and Wild 2 particles: from Antarctic snow to cometary ices. *Meteorit. Planet. Sci.* **44**, 1643–1661.

Dodony I. and Posfai M. (1990) Pyrrhotite superstructures. Part II: A TEM study of 4C and 5C structures. *Eur. J. Mineral.* **2**, 529–535.

Engrand C., Duprat J., Maurette M. and Gounelle M. (2007) Fe–Ni sulfides in concordia antarctic micrometeorites. *Lunar Planet. Sci. XXXVIII*. Lunar Planet. Inst., Houston. #1668 (abstr.).

Fink U., Hicks M. P. and Fevig R. A. (1999) Production rates for the Stardust mission target: comet 81P/Wild 2. *Icarus* **141**, 331–340.

Fitch F., Schwarcz H. P. and Anders E. (1962) *Organized elements in carbonaceous chondrites. In Life-forms in Meteorites – A Symposium*. Macmillan Journals, London.

Fleet M. E. (1968) On the lattice parameters and superstructure of pyrrhotites. *Am. Mineral.* **53**, 1846–1855.

Fleet M. E. (1971) Refinement of crystal structure of cubanite and polymorphism of $CuFe_2S_3$. *Z. Kristallogr. Krist.* **132**, 276–287.

Flynn G. J., Bleuet P., Borg J. and 77 Others (2006) Elemental compositions of comet 81P/Wild 2 samples collected by Stardust. *Science* **314**, 1731–1735.

Flynn G., Leroux H., Tomeoka K., Tomioka N., Ohnishi I., Mikouchi T., Wirick S., Keller L. P., Jacobsen C. and Sandford S. A. (2008) Carbonate in comets: a comparison of comets 1P/Halley, 9P/Temple 1, and 81P/Wild 2. *Lunar Planet. Sci. XXXIX*. Lunar Planet. Inst., Houston. #1979 (abstr.).

Flynn G., Wirick S., Keller L. P. and Jacobsen C. (2009) STXM search for carbonate in samples of comet 81P/Wild 2. *J. Phys. Conf. Ser.* **186**, 012085.

Foster N. J., Kearsley A., Burchell M., Wozniakiewicz, P., Creighton, J. A. and Cole, M. J. (2008) Analysis of hydrous phyllosilicates in Stardust type B track analogues. *Asteroids, Comets, Meteors X*. Lunar Planet. Inst., Houston. #8209 (abstr.).

Fredriksson K. and Kerridge J. F. (1988) Carbonates and sulfates in CI Chondrites – formation by aqueous activity on the parent body. *Meteoritics* **23**, 35–44.

Gounelle M. and Zolensky M. E. (2001) A terrestrial origin for sulfate veins in CI1 chondrites. *Meteorit. Planet. Sci.* **36**, 1321–1329.

Greshake A., Flynn G. and Bajt S. (1997) Trace element concentrations in pyrrhotites from Orgueil (CI). *Lunar Planet. Sci. XXVIII*. Lunar Planet. Inst., Houston. #1344 (abstr.).

Hall H. T. and Yund R. A. (1966) Pyrrhotite phase relations below 325 °C. *Econ. Geol.* **61**, 1297.

Herndon J. M., Rowe M. W., Larson E. E. and Watson D. E. (1975) Origin of magnetite and pyrrhotite in carbonaceous chondrites. *Nature* **253**, 516–518.

Hersant F., Gautier D. and Hure J.-M. (2001) A two-dimensional model for the primordial nebula constrained by D/H measurements in the solar system: Implications for the formation of giant planets. *Astrophys. J.* **554**, 391–407.

Hoppe P., Macdougall D. and Lugmair G. W. (2008) Extinct manganese-53 in carbonates from the Orgueil meteorite. *New Astro. Rev.* **52**, 467–470.

Hubickyj O., Bodenheimer P. and Lissauer J. J. (2005) Accretion of the gaseous envelope of Jupiter around a 5–10 Earth–mass core. *Icarus* **179**, 415–431.

Ishii H. A., Bradley J. P., Dai Z. R., Chi M. F., Kearsley A. T., Burchell M. J., Browning N. D. and Molster F. (2008) Comparison of comet 81P/Wild 2 dust with interplanetary dust from comets. *Science* **319**, 447–450.

Kaneda H., Shoji T. and Takenouchi S. (1978) Heating experiments of cubanite. *Kozan Chishitsu* = *Mining Geology* **28**, 71–82.

Keller L. P., Bajt S., Baratta G. A. and 30 Others (2006) Infrared spectroscopy of comet 81P/Wild 2 samples returned by Stardust. *Science* **314**, 1728–1731.

Kerridge J. F. (1970) Meteoritic pyrrhotite. *Meteoritics* **5**, 149–152.

Kerridge J. F. and Chatterji S. (1968) Magnetite content of a type 1 carbonaceous meteorite. *Nature* **220**, 775.

Kerridge J. F., Fredriksson K., Jarosewich E., Nelen J. and Macdougall J. D. (1980) Carbonates in CI chondrites. *Meteoritics* **15**, 313–314.

Kerridge J. F., Macdougall J. D. and Marti K. (1979) Clues to the origin of sulfide minerals in Cl chondrites. *Earth Planet. Sci. Lett.* **43**, 359–367.

Kullerud G., Yund R. A. and Moh G. H. (1969) Phase relations in the Cu–Fe–S, Cu–Ni–S, and Fe–Ni–S systems. In *Magmatic Ore Deposits: A symposium* (ed. H. D. B. Wilson). Economic Geology Publishing Co., Lancaster. pp. 344–358.

Lauretta D. S. (2005) Sulfidation of an iron–nickel–chromium–cobalt-phosphorus alloy in 1% H2S–H2 gas mixtures at 400–1000 °C. *Oxid. Met.* **64**, 1–22.

Lauretta D. S., Devouard B. and Buseck P. R. (1999) The cosmochemical behavior of mercury. *Earth Planet. Sci. Lett.* **171**, 35–47.

Lauretta D. S., Fegley B., Lodders K. and Kremser D. T. (1996a) The kinetics and mechanism of iron sulfide formation in the solar nebula. *Proceedings of the NIPR Symposium on Antarctic Meteorites* **6**, 111–126.

Lauretta D. S., Kremser D. T. and Fegley B. (1996b) The rate of iron sulfide formation in the solar nebula. *Icarus* **122**, 288–315.

Lauretta D. S., Lodders K. and Fegley B. (1997) Experimental simulations of sulfide formation in the solar nebula. *Science* **277**, 358–360.

Lauretta D. S., Lodders K. and Fegley B. (1998) Kamacite sulfurization in the solar nebula. *Meteorit. Planet. Sci.* **33**, 821–833.

Leroux H., Rietmeijer F. J. M., Velbel M., Brearley A., Jacob D., Langenhorst F., Bridges J. C., Zega T., Stroud R., Cordier P., Harvey R., Lee M., Gounelle M. and Zolensky M. (2008) Study of thermally modified comet 81P/Wild 2 dust particles by interactions with the aerogel matrix during the Stardust capture process. *Meteorit. Planet. Sci.* **43**, 97–120.

Leroux H., Roskosz M. and Jacob D. (2009) Oxidation state of iron and extensive redistribution of sulfur in thermally modified Stardust particles. *Geochim. Cosmochim. Acta* **73**, 767–777.

Lewis J. S. (2004) *Physics and Chemistry of the Solar System*. Elsevier Academic Press, Burlington.

Liou J. C. and Zook H. A. (1996) Comets as a source of low eccentricity and low inclination interplanetary dust particles. *Icarus* **123**, 491–502.

Lissauer J. J., Hubickyj O., D'Angelo G. and Bodenheimer P. (2009) Models of Jupiter's growth incorporating thermal and hydrodynamic constraints. *Icarus* **199**, 338–350.

Lisse C. M., VanCleve J., Adams A. C., A'Hearn M. F., Fernandez Y. R., Farnham T. L., Armus L., Grillmair C. J., Ingalls J., Belton M. J. S., Groussin O., McFadden L. A., Meech K. J., Schultz P. H., Clark B. C., Feaga L. M. and Sunshine J. M. (2006) Spitzer spectral observations of the deep impact ejecta. *Science* **313**, 635–640.

Lodders K. (2003) Solar system abundances and condensation temperatures of the elements. *Astrophys. J.* **591**, 1220–1247.

Macdougall J. D. and Kerridge J. F. (1977) Cubanite – new sulfide phase in CI meteorites. *Science* **561**, 562.

MacPherson G. J., Bullock E. S., Janney P. E., Kita N. T., Ishikubo T., Davis A. M., Wadhwa M. and Krot A. N. (2010) Early solar nebula condensates with canonical, not supracanonical initial $^{26}Al/^{27}Al$ ratios. *Astrophys. J. Lett.* **711**, L117–L121.

Makovicky E. (2006) Crystal structures of sulfides and other chalcogenides. In *Reviews in Mineralogy and Geochemistry: Sulfide Mineralogy and Geochemistry* (ed. D. J. Vaughan). Mineralogical Society of America, Chantilly. pp. 7–126.

McSween H. Y. and Weissman P. R. (1989) Cosmochemical implications of the physical processing of cometary nuclei. *Geochim. Cosmochim. Acta* **53**, 3263–3271.

Nakamura T., Tsuchiyama A., Akaki T., Uesugi K., Nakano T., Takeuchi A., Suzuki Y. and Noguchi T. (2008) Bulk mineralogy and three-dimensional structures of individual Stardust particles deduced from synchrotron X-ray diffraction and microtomography analysis. *Meteorit. Planet. Sci.* **43**, 247–259.

Naldrett A. J. (1989) *Magmatic Sulfide Deposits*. Oxford University Press, New York.

O'Reilly W., Hoffmann V., Chouker A. C., Soffel H. C. and Menyeh A. (2000) Magnetic properties of synthetic analogues of pyrrhotite ore in the grain size range 1–24 μm. *Geophys. J. Int.* **142**, 669–683.

Pasek M. A., Milsom J. A., Ciesla F. J., Lauretta D. S., Sharp C. M. and Lunine J. I. (2005) Sulfur chemistry with time-varying oxygen abundance during solar system formation. *Icarus* **175**, 1–14.

Pearson A. D. and Buerger M. J. (1956) Confirmation of the crystal structure of pentlandite. *Am. Mineral.* **41**, 804–805.

Posfai M. and Buseck P. R. (1997) Modular structures in sulphides: sphalerite/wurtzite-, pyrite/marcasite-, and pyrrhotite-type minerals. In *EMU Notes in Mineralogy: Modular Aspects of Minerals* (ed. S. Merlino). Eotvos University Press. pp. 193–235.

Posfai M. and Dodony I. (1990) Pyrrhotite superstructures. Part I: fundamental structures of the NC ($N = 2$, 3, 4 and 5) type. *Eur. J. Mineral.* **2**, 525–528.

Posfai M., Sharp T. G. and Kontny A. (2000) Pyrrhotite varieties from the 9.1 km deep borehole of the KTB project. *Am. Mineral.* **85**, 1406–1415.

Pruseth K. L., Mishra B. and Bernhardt H. J. (1999) An experimental study on cubanite irreversibility: implications for natural chalcopyrite–cubanite intergrowths. *Eur. J. Mineral.* **11**, 471–476.

Putnis A. (1975) Observations on coexisting pyrrhotite phases by transmission electron microscopy. *Contrib. Mineral. Petr.* **52**, 307–313.

Putnis A. (1977) Electron-microscope study of phase-transformations in cubanite. *Phys. Chem. Miner.* **1**, 335–349.

Rietmeijer F. (2004) Dynamic pyrometamorphism during atmospheric entry of large (10 μm) pyrrhotite fragments from cluster IDPs. *Meteorit. Planet. Sci.* **39**, 1869–1887.

Rietmeijer F. J. M., Nakamura T., Tsuchiyama A., Uesugi K., Nakano T. and Leroux H. (2008) Origin and formation of iron silicide phases in the aerogel of the Stardust mission. *Meteorit. Planet. Sci.* **43**, 121–134.

Stodolna J., Jacob D. and Leroux H. (2009) A TEM study of four particles extracted from the Stardust track 80. *Meteorit. Planet. Sci.* **44**, 1511–1518.

Stodolna J., Jacob D. and Leroux H. (2010) Mineralogy of Stardust track 80: evidence for aqueous alteration and igneous processes. *Lunar Planet. Sci. XLI*. Lunar Planet. Inst., Houston. #1657 (abstr.).

Sugaki A. and Shima H. (1965) Synthetic sulfide minerals (III). *Memoirs of the Faculty of Engineering, Yamaguchi University* **16**, 109–118.

Szymanski J. T. (1974) A refinement of structure of cubanite, $CuFe_2S_3$. *Z. Kristallogr.* **140**, 218–239.

Tokonami M., Nishiguchi K. and Morimoto N. (1972) Crystal structure of a monoclinic pyrrhotite (Fe_7S_8). *Am. Mineral.* **57**, 1066–1080.

Tomeoka K. and Buseck P. R. (1984) Transmission electron microscopy of "LOW-CA" hydrated interplanetary dust particle. *Earth Planet. Sci. Lett.* **69**, 243–254.

Tomeoka K. and Buseck P. R. (1988) Matrix mineralogy of the Orgueil CI carbonaceous chondrite. *Geochim. Cosmochim. Acta* **52**, 1627–1640.

Tomeoka K., Tomioka N. and Ohnishi I. (2008) Silicate minerals and Si–O glass in comet Wild 2 samples: Transmission electron microscopy. *Meteorit. Planet. Sci.* **43**, 273–284.

Vaughan D. J. and Craig J. R. (1997) Sulfide ore mineral stabilities, morphologies, and intergrowth textures. In *Geochemistry of Hydrothermal Ore Deposits, Third Edition* (ed. H. L. Barnes). John Wiley and Sons, New York. pp. 367–434.

Velbel M. A. and Harvey R. P. (2009) Along-track compositional and textural variation in extensively melted grains returned from comet 81P/Wild 2 by the Stardust mission: implications for capture-melting process. *Meteorit. Planet. Sci.* **44**, 1519–1540.

Wang H., Pring A., Wu F., Chen G., Jiang J., Xia F., Zhang J., Ngothai Y. and O'Neill B. (2006) Effect of cation vacancy and crystal superstructure on thermodyanmics of iron monosulfides. *J. Sulfur Chem.* **27**, 271–282.

Weisberg M., McCoy T. J. and Krot A. (2006) Systematics and evaluation of meteorite classification. In *Meteorites and the Early Solar System II* (eds. D. S. Lauretta and H. Y. McSween). University of Arizona Press, Tucson. pp. 19–52.

Wirick S., Leroux H., Tomeoka K., Zolensky M., Flynn G., Tyliszczak T., Butterworth A., Tomioka N., Ohnishi I., Nakamura-Messenger K., Sandford S. A., Keller L. P. and Jacobsen, C. (2007) Carbonate found in Stardust aerogel tracks. *Lunar Planet. Sci. XXXVIII*. Lunar Planet. Inst., Houston. #1534 (abstr.).

Wozniakiewicz P. J., Ishii H. A., Kearsley A. T., Burchell M. J., Bradley J. P., Teslich N. and Cole M. J. (2010) Survivability of cometary phyllosilicates in Stardust collections and implications for the nature of comets. *Lunar Planet. Sci. XLI*. Lunar Planet. Inst., Houston. #2357 (abstr.).

Yund R. A. and Hall H. T. (1969) Hexagonal and monoclinic pyrrhotites. *Econ. Geol.* **64**, 420–423.

Yund R. A. and Kullerud G. (1966) Thermal stability of assemblages in Cu–Fe–S system. *J. Petrol.* **7**, 454.

Zega T. J., Nittler L. R., Busemann H., Hoppe P. and Stroud R. M. (2007) Coordinated isotopic and mineralogic analyses of planetary materials enabled by in situ lift-out with a focused ion beam scanning electron microscope. *Meteorit. Planet. Sci.* **42**, 1373–1386.

Zolensky M. E., Bourcier W. L. and Gooding J. L. (1989) Aqueous alteration on the hydrous asteroids – results of Eq3/6 computer simulations. *Icarus* **78**, 411–425.

Zolensky M. E., Krot A. N. and Benedix G. (2008a) Record of low-temperature alteration in asteroids. *Rev. Mineral. Geochem.* **68**, 429–462.

Zolensky M., Nakamura-Messenger K., Rietmeijer F. J. M. and 28 Others (2008b) Comparing Wild 2 particles to chondrites and IDPs. *Meteorit. Planet. Sci.* **43**, 261–272.

Zolensky M. E. and Thomas K. L. (1995) Iron and iron–nickel sulfides in chondritic interplanetary dust particles. *Geochim. Cosmochim. Acta* **59**, 4707–4712.

Zolensky M. E., Zega T. J., Yano H. and 72 Others (2006) Report – mineralogy and petrology of comet 81P/Wild 2 nucleus samples. *Science* **314**, 1735–1739.

Associate editor: Sara S. Russell